

A new catalogue of head-tail radio galaxies from LoTSS DR1

Sabyasachi Pal^{*1} Shobha Kumari¹

¹Midnapore City College, Kuturia, Bhadutala, Paschim Medinipur, West Bengal, 721129, India

Accepted 03 Aug 2022. Revised 19 Jul 2022. In original form 20 May 2022.

^{*}Corresponding author. E-mail: sabya.pal@gmail.com (SP)

Abstract. The unique morphology of head-tail (HT) radio galaxies suggests that radio jets and their intra-cluster medium interact strongly. We conducted a systematic search for HT radio galaxies using the LOFAR Two-metre Sky Survey first data release (LoTSS DR1) at 144 MHz. In this paper, a catalogue of fifty-five new HT radio galaxies is presented, ten of which are narrow-angle tailed sources (NATs) and forty-five of which are wide-angle tailed sources (WATs). NATs are characterised by tails that are bent like a narrow ‘V’ shape with a less than 90 degree opening angle. The opening angle between jets in WAT radio galaxies is greater than ninety degrees, exhibiting wide ‘C’-like morphologies. We found that thirty out of fifty-five HT radio galaxies reported in this article are associated with known galaxy clusters. Most of the sources presented in the current paper have redshifts < 0.5 . The various physical properties and statistical studies of these HT radio galaxies are presented.

Keywords. galaxies: active – galaxies: jets – quasars: general – radio continuum: galaxies.

1. Introduction

The head-tail (HT) morphology of radio galaxies is determined by radio jets that appear to bend in a common direction, resembling a tail, with the luminous host galaxy acting as ‘head’. This class of radio sources is also widely recognized as C-shaped radio sources or bent radio sources or Bend-Tail radio sources in general (Ryle & Windram, 1968; Rudnick & Owen, 1976; Blanton *et al.*, 2000; Proctor, 2011; Dehghan *et al.*, 2014) and this type of radio source was first mentioned by Ryle & Windram (1968). These radio galaxies are classified into two categories based on their degree of bending and luminosity, namely wide-angle tailed (WAT) radio sources and narrow-angle tailed (NAT) radio sources (Owen & Rudnick, 1976). 3C 465 is known as the prototype for the WAT class radio sources (Eilek *et al.*, 1984; Eilek & Owen, 2002; Hardcastle, Sakellou & Worrall, 2005).

Initially, WATs were thought to be an extension of the HT subclass because of the large opening angles between their tails (Rudnick & Owen, 1976). WATs now include HT as well as objects with an opening angle greater than 90° (Rudnick & Owen, 1977; Mingo *et al.*, 2019). NATs are defined as objects with opening angles of less than 90° (Mingo *et al.*, 2019). These types of sources are most commonly found in the clus-

ter of galaxy and thus they can serve as galaxy cluster tracers (Mao *et al.*, 2010). In the local Universe (up to $z = 1$), Blanton *et al.* (2003) detected galaxy clusters by using HT radio galaxies. In addition, Dehghan *et al.* (2014) discovered more distant clusters up to $z = 2$. WAT sources are thought to be a sub-population of FR-Is (Mingo *et al.*, 2019).

According to a recent study on 47 WATs, it is found that these sources are located in the region of the modified Owen-Ledlow diagram where FR-Is are most densely populated (Missaglia *et al.*, 2019; Bhukta, Pal & Mondal, 2022). The spectroscopic classification indicated that all detected FR-Is were low-excitation radio galaxies (LERGs). However, a multifrequency comparative study of WATs with detected FR-Is and FR-IIs at the same redshifts showed that the multifrequency properties of WATs were remarkably similar to FR-I radio galaxies and had radio powers typical of FR-IIs (Missaglia *et al.*, 2019). Further study is needed to find whether WATs should be regarded as a subset of FR-Is or as a distinct class in their own right.

What governs the formation of these very distinct morphologies is still unknown. Jets in HT radio galaxies are thought to be caused by two potential mechanisms related to the velocity of the host galaxy in the intra-cluster medium (ICM). 1) The velocity of the host galaxy is unusually higher than expected, resulting in

ram pressure on the jets (Miley *et al.*, 1972; Rudnick & Owen, 1976), where ram pressure, P_{ram} , is defined as

$$P_{ram} \propto \rho v^2 \quad (1)$$

where ρ is the density of the ICM, and v is the velocity between the galaxy and the ICM (Gunn & Gott, 1972). 2) ‘Cluster weather’ is responsible for the formation of these types of radio galaxies (Burns, 1998). Dynamical interactions, such as cluster–cluster mergers or group accretion onto clusters, are thought to influence the bending of the jets in the ICM. It is believed that NATs form as a result of ram pressure on the jets by the host galaxy when the host galaxy acquires a higher velocity (in the order of 600 km s^{-1}) than the expected velocity (Venkatesan *et al.*, 1994) whereas WATs are thought to be formed by ‘cluster weather’ (Klamer, Subrahmanyan & Hunstead, 2004).

NGC 1265 is the most commonly used prototype of a NAT radio source (Ryle & Windram, 1968; O’Dea & Owen, 1986). Recently, with the help of the Tata Institute of Fundamental Research (TIFR) Giant Metrewave Radio Telescope (GMRT) Sky Survey Alternative Data Release 1 (TGSS ADR 1; (Intema *et al.*, 2017)), Bhukta, Pal & Mondal (2022) presented 265 HT radio galaxies (204 are WATs and 61 are NATs). Using the Australia Telescope Large Area Survey of the South Pole Telescope Spitzer Deep Field (ATLAS-SPT), O’Brien *et al.* (2018) presented a sample of 24 sources with HT morphology. A Multi-frequency study of an interacting narrow-angle tail radio galaxy J0037+18 was done by Patra *et al.* (2019). With the Australia Telescope Large Area Survey (ATLAS) of the Chandra Deep Field South, Dehghan *et al.* (2014) detected 55 HT radio galaxies. With the help of the VLA FIRST survey, Missaglia *et al.* (2019) and Sasmal *et al.* (2022) reported 47 and 717 (287 NAT and 430 WAT) HT radio galaxies, respectively. Piffaretti *et al.* (2011) catalogued a list of radio sources via automated pattern recognition algorithms using NVSS. From the listed catalogues of Piffaretti *et al.* (2011), Yu-Xing *et al.* (2019) confirmed 412 HT radio galaxies.

In this paper, we report a systematic finding of 55 HT radio galaxies from the high-resolution Low-Frequency Array (LOFAR) Two-metre Sky Survey first data release (LoTSS DR1). In Section 2., we describe our search methodology, which includes a description of the LoTSS survey, the search strategy, the definition of WATs and NATs, and the respective optical counterpart of each source. In the next section (section 3.), we summarise the result. In the last section (section 4.), we made a discussion on the findings. We have used the following cosmological parameters in this paper from the final full-mission Planck measurements of the cosmic microwave background anisotropies, com-

binning information from the temperature and polarisation maps and the lensing re-construction; $H_0 = 67.4 \text{ km s}^{-1} \text{ Mpc}^{-1}$, $\Omega_m = 0.315$ and $\Omega_{vac} = 0.685$ (Aghanim *et al.*, 2020).

2. Methodology

2.1 LoTSS DR1

LOFAR is currently the largest ground-based radio telescope operating in the low-frequency range of 120–168 MHz. Unlike a single-dish telescope, LOFAR is a multipurpose sensor network, with an innovative computer and network infrastructure that can handle extremely large data volumes. LOFAR Two-metre Sky Survey first data release (LoTSS DR1) covers 424 square degrees of radio sky in the HETDEX spring field region, accounting for about 2 per cent of the total LoTSS coverage (Shimwell *et al.*, 2019). It is an ongoing survey that aims to cover the entire northern sky. We used this survey at a frequency of 144 MHz to detect HT radio galaxies in the covered region. The DR1 data release includes right ascension (RA) ranges from 10h45m00s to 15h30m00s and declination (DEC) from $45^\circ 00' 00''$ to $57^\circ 00' 00''$. The survey images are developed by using a fully automated, direction-dependent calibration and imaging pipeline. The survey has a median sensitivity of $S_{144} = 71 \mu\text{Jy beam}^{-1}$ and the point-source completeness of the survey is 90 per cent at an integrated flux density of 0.45 mJy. The angular resolution of the images is $6''$ (Shimwell *et al.*, 2019).

At 1.4 GHz, there are two high-frequency sky surveys: a) the NRAO VLA Sky Survey (NVSS) with a VLA D configuration that covers 82 per cent of the celestial sphere with an rms of $\sim 0.45 \text{ mJy}$ and an angular resolution of $45''$ (Condon *et al.*, 1998). b) Faint Images of the Radio Sky at Twenty-Centimeters (FIRST) with VLA B configuration, has an angular resolution of $5''$ and a typical rms of 0.15 mJy (Becker *et al.*, 1995). Due to limited resolution, high-sensitive NVSS is suitable to detect large-scale diffuse emissions but can not reveal finer details in galaxy morphology. The high-resolution FIRST survey, on the other hand, can provide more information about the core but is not good for detecting large-scale diffuse emissions. LoTSS data with high sensitivity and high resolution provides more information about large-scale diffuse emission as well as detailed information about galaxy morphology. Taking advantage of 50–1000 times better sensitivity and 5–30 times higher resolution in comparison to other low-frequency wide-area surveys (like GLEAM; (Wayth *et al.*, 2015), TGSS; (Intema *et al.*, 2017), MESS; (Heald *et al.*, 2015) and VLSSr; (Lane *et al.*, 2014)), LoTSS DR1 could be used to look for a variety of radio sources.

Recently, using this survey, [Pal & Kumari \(2021\)](#) listed 33 winged radio galaxies. 459 HT radio galaxies were also reported using this survey by [Mingo *et al.* \(2019\)](#).

2.2 Search strategy

LoTSS DR1 includes a total of 325,694 sources with a 5σ detection limit. The source density in LoTSS is a factor of 10 times higher than the most sensitive existing very wide-area radio-continuum surveys ([Shimwell *et al.*, 2019](#)). Using this survey, we aimed to find HT radio galaxies. To identify a list of HT radio galaxies, we filtered the sources in the catalogue with angular sizes $\geq 12''$ (i.e. at least twice the convolution beam size), which yielded 18,500 sources. We visually inspected the fields of all of these 18500 sources in search of a new finding for HT radio galaxies. We categorized the list of sources on the basis of bending angle. We removed sources with larger bending angles ($>160^\circ$) and listed only those sources whose bending angles are $\leq 160^\circ$.

We cross-matched the list of sources presented in this paper with previously reported HT radio galaxies by [Mingo *et al.* \(2019\)](#); [Sasmal *et al.* \(2022\)](#). From our catalogue, we removed all the HT radio galaxies that were previously reported by [Mingo *et al.* \(2019\)](#) and we also removed one HT radio galaxy (J1242+5021), as this source is already listed by [Sasmal *et al.* \(2022\)](#). Out of fifty-five listed sources in this current paper, [Mingo *et al.* \(2019\)](#) catalogued thirty-six sources without classifying them as HT radio galaxies.

2.3 Optical counterparts

In the current paper, we searched for optical counterparts for all the reported HT galaxies using the Sloan Digital Sky Survey (SDSS) data catalogue ([Gunn *et al.*, 2006](#)). The optical counterparts of these galaxies are marked with \times in Figs. 1 and 2. Out of 55 newly discovered HT radio galaxies, optical counterparts are found for 44 HT radio galaxies. For some HT radio galaxies, their optical counterparts are not detected. In those cases, we used our best-guess eye estimated (EE) position as the position of HT radio galaxies. Sources with no optical counterparts are marked with $*$ in the table 1 and 2.

2.4 Definition of the NAT and WAT sources

We identified HT radio galaxies by manually inspecting all extended sources ($\geq 12''$) in the LoTSS DR1 survey. HT radio galaxies exhibit significant jet bending apart from the typical linear trajectory. The HT radio galaxies are classified into two sub-classes based on the angle of bending between the two radio jets: wide angle tail (WAT) and narrow-angle tail (NAT). WATs

are defined as sources with bending angle $\geq 90^\circ$ while sources with an angle of less than 90° are termed NAT sources. The bending angle is measured by drawing two straight lines parallel to the two opposite sides of radio jets emanating from the core of the galaxy (optical counterpart). It should be noted that a particular WAT source may appear as a NAT source on our radio map due to the projection effect or the orientation to the plane of the sky.

3. Result

3.1 Source catalogue

We discovered fifty-five new HT radio galaxies using LoTSS DR1, among which 45 are WAT sources and 10 are NAT sources. In Tables 1 and 2, we tabulated a list of 45 WATs and 10 NATs. Columns (3) and (4) showed the Right Ascension (J2000.0) and Declination (J2000.0) of HT radio galaxies. We used the best location of the optical host galaxy from SDSS as the location of the HT source when the optical host galaxy is available.

The redshift of the host galaxy is mentioned in column (5), when available. In column (6), we measured flux density at 144 MHz in mJy (F_{144}) using LoTSS DR1. The flux density at 1400 MHz, measured by NVSS, is mentioned in column (7). The spectral indices between 144 MHz and 1400 MHz are mentioned in column (8) (discussed in detail in Section 3.3) and the radio luminosity in column (9) (discussed in detail in Section 3.4).

3.2 Angle between two jets of HT radio galaxies

The opening angle of jets is measured for the WAT and NAT sources presented in the current paper. The opening angle is measured using the peak points in both the lobes and the core of the galaxy. The extreme bending NAT radio galaxy is J1506+5311 with a bending angle of 40° and the lowest bending WAT radio galaxy is J1523+5255 with a bending angle of 160° . In Fig. 3, a histogram with the opening angle distribution of WAT and NAT sources is shown. The histogram showed a peak between the angles of 120° to 130° . Because of the complex structure of some of the sources, the bending angle could not be measured. It should be noted that sources with very small bending are not catalogued, so there might be a possibility of bias in this angle distribution diagram.

3.3 Spectral index

The two-point spectral index (α_{1400}^{144}) of newly discovered HT radio galaxies is measured using NVSS (at 1400 MHz) and LoTSS (at 144 MHz), under the assumption of $S \propto \nu^{-\alpha}$, where α is the spectral index and S is the radiative flux density at a given frequency (ν). In Fig. 4, a histogram showing the spectral index (α_{1400}^{144}) distribution of 45 WATs and 10 NATs, reported in the current paper, is shown. We also included 204 WATs and 61 NATs from Bhukta, Pal & Mondal (2022) in the histogram.

The histogram showed a peak near $\alpha_{1400}^{144} = 0.80$. The total span of α_{1400}^{144} is from 0.22 to 0.79 for NAT sources and from 0.41 to 1.57 for WAT sources. For NAT sources, J1505+4706 has the lowest spectral index with $\alpha_{1400}^{144} = 0.22$ and J1207+4805 has the highest spectral index with $\alpha_{1400}^{144} = 0.79$. For WAT sources, J1325+5617 has the lowest spectral index with $\alpha_{1400}^{144} = 0.41$ and J1224+4905 has the highest spectral index with $\alpha_{1400}^{144} = 1.57$. None of the HT radio galaxies has an inverted spectrum.

3.4 Radio luminosity

The radio luminosities (L_{rad}) of WAT and NAT sources are measured (when the value of z is available) using the standard formula (Donoso, Best & Kauffmann, 2009)

$$L_{\text{rad}} = 4\pi D_L^2 S (1+z)^{\alpha-1} \quad (2)$$

where D_L is luminosity distance to the source in metre (m), α is the spectral index ($S \propto \nu^{-\alpha}$), z is the redshift of the radio galaxy, and S is the flux density ($\text{W m}^{-2} \text{Hz}^{-1}$) at a given frequency. In column 9 of Table 1 and 2, the luminosities of sources are shown. The range of $\log L_{\text{rad}}$ in the present sample is 24.47 to 26.35. The most luminous NAT source in the present sample is J1207+4805 with a $\log L_{\text{rad}} = 26.31$ and the most luminous WAT source is J1049+4619 with a $\log L_{\text{rad}} = 26.35$. The least luminous NAT source in the present sample is J1506+5311 with a $\log L_{\text{rad}} = 25.21$ and the least luminous WAT source is J1115+4834 with a $\log L_{\text{rad}} = 24.47$.

3.5 Possible radio relics

Radio relics are synchrotron-derived diffuse, elongated radio emitters that are frequently observed in galaxy clusters without an apparent host galaxy. It is believed that radio relics are traces of shock wave generation during the merger of galaxy clusters (Fernández et al., 2021). These objects may either have no AGN activity or activity that is so weak that outflowing jets can no

longer be sustained or maybe at the final stage of radio source evolution (Tamhane et al., 2015).

Radio relics have been observed in clusters like Coma, Abell 2255, and Abell 2256 with sizes ≥ 1 Mpc. It is found that in some of the cases (MACS J1752.0+4440 (van Weeren et al., 2012; Bonafede et al., 2012), PSZ1 G108.18–11.53 (de Gasperin et al., 2015), and CIZA J2242.8+5301 (van Weeren et al., 2010)), two radio relics were observed in the same cluster, usually running parallel to the distribution of ICM. The cluster Abell 3667, Abell 2345, Abell 1240, as well as ZwCl 0008.8+5215, and ZwCl 2341.1+0000, comprise two very luminous, virtually similar relics in a distance of larger than 5 Mpc (Willis, Strom & Wilson, 1974; Cordey, 1987; Vessey & Green, 1998; Murgia et al., 2011; Tamhane et al., 2015; Hurley-Walker et al., 2015).

We reported four sources (J1147+5548, J1346+5250, J1347+5022, and J1510+5146), with HT-like morphology (2 WATs and 2 NATs) which have no optical counterparts but are associated with known clusters (WHL J114703.7+554715, MaxBCG J206.50836+52.82084, WHL J134708.2+502222, and WHL J151003.4+514612, respectively). These extended bend sources could be radio relics.

4. Discussion

4.1 Radio properties of HT radio galaxies

Radio galaxies can be distinguished by their radio properties such as spectral index, radio luminosity, angular size, and linear size with respect to their measured spectroscopic redshifts. Among 55 HT radio galaxies presented in the current paper, redshifts are found for 26 HT radio galaxies (48 per cent) from the SDSS catalogue, with 5 NATs and 21 WATs. All 26 HT radio galaxies have spectroscopic redshifts. The majority of detected sources have redshift $z \leq 0.5$. Two NATs (J1132+5459 and J1147+4805) have redshifts $z > 0.5$. J1147+4805 is the furthest NAT with a redshift of $z = 0.70$. Only one WAT source, J1113+4952, has redshift $z > 0.5$ ($z = 0.61$, the furthest source in the present paper). The nearest WAT source in our sample is J1115+4834 with $z = 0.07$. Previously, in the HT catalogue of Misaglia et al. (2019), sources had redshift $z \leq 0.15$. Two sixty-five (204 WATs and 61 NATs) HT radio galaxies were presented by Bhukta, Pal & Mondal (2022), also had a redshift in the range of 0.01–0.68 in which only four sources had a redshift $z \geq 0.5$. This can be concluded that the majority of HT radio galaxies are found in low redshift regions.

The spectral indices for the presented sources in the current paper are listed in the tables 1 and 2.

The average spectral index for WATs in the current

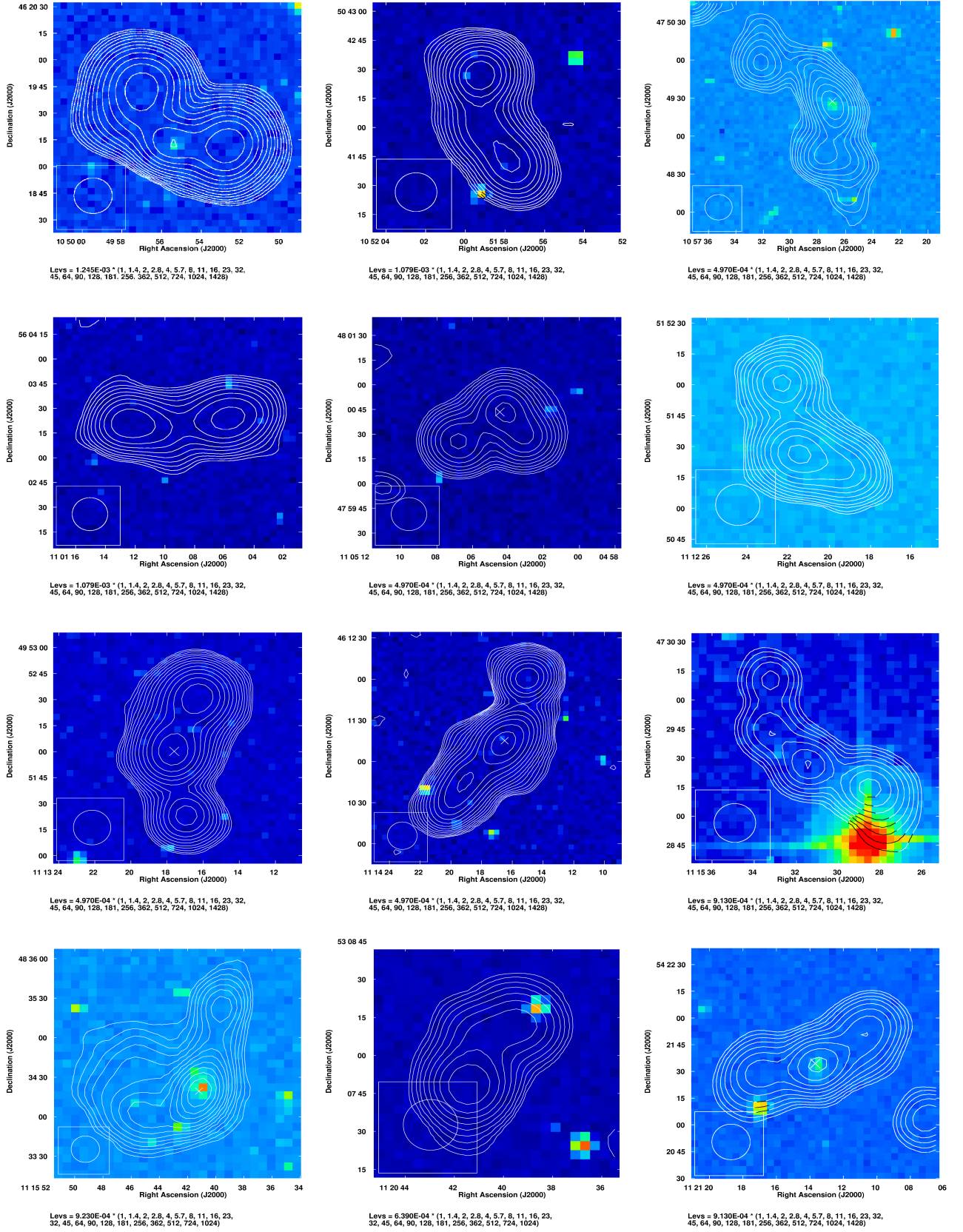


Figure 1. LOFAR images of WAT radio galaxies (contours) overlaid on DSS2 red images (colour). Here white cross mark represent the optical counterpart for the sources, when available.

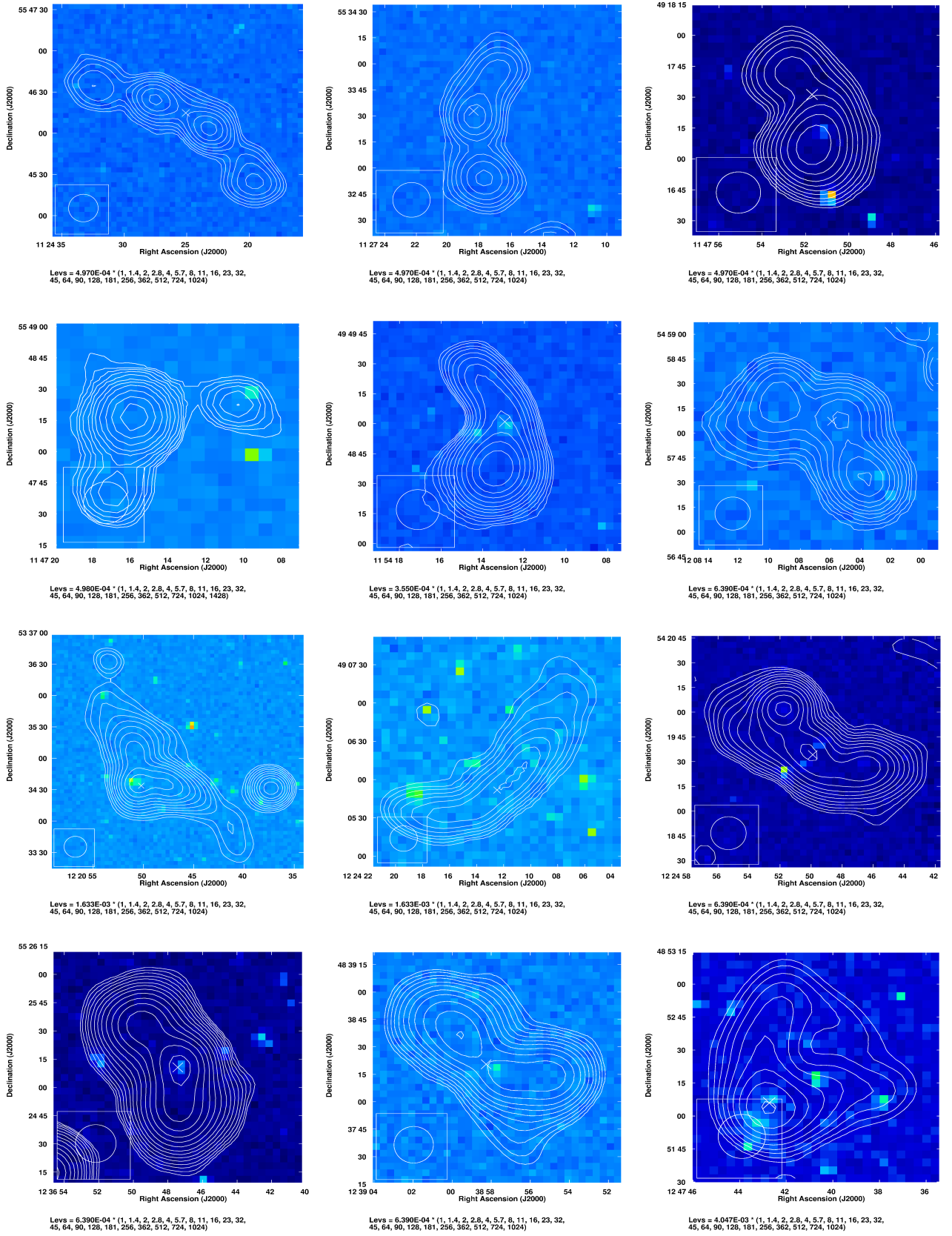


Figure 1. LOFAR images of WAT radio galaxies (contours) overlaid on DSS2 red images (colour). Here white cross mark represent the optical counterpart for the sources, when available.

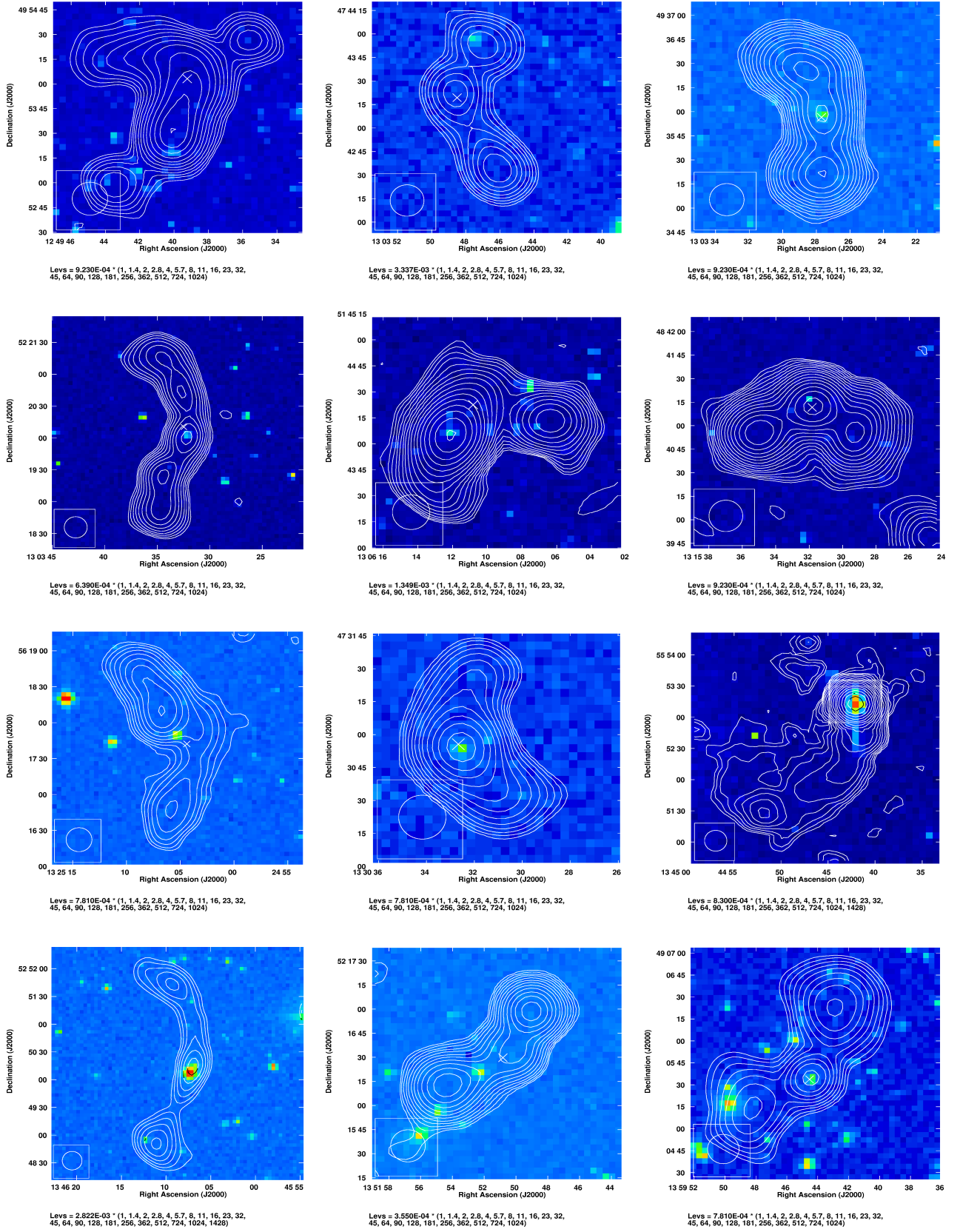


Figure 1. LOFAR images of WAT radio galaxies (contours) overlaid on DSS2 red images (colour). Here white cross mark represent the optical counterpart for the sources, when available.

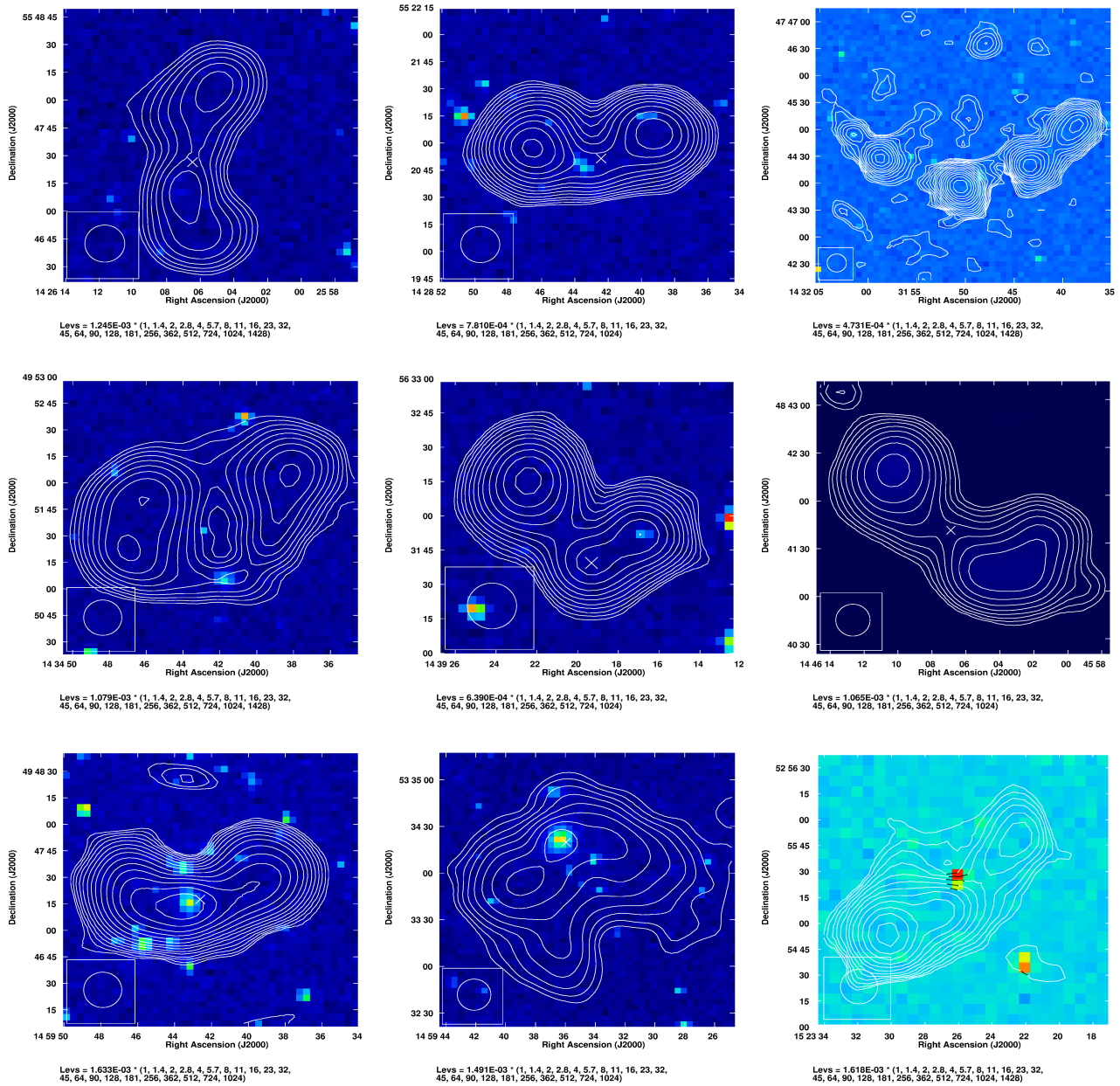


Figure 1. LOFAR images of WAT radio galaxies (contours) overlaid on DSS2 red images (colour). Here white cross mark represent the optical counterpart for the sources, when available.

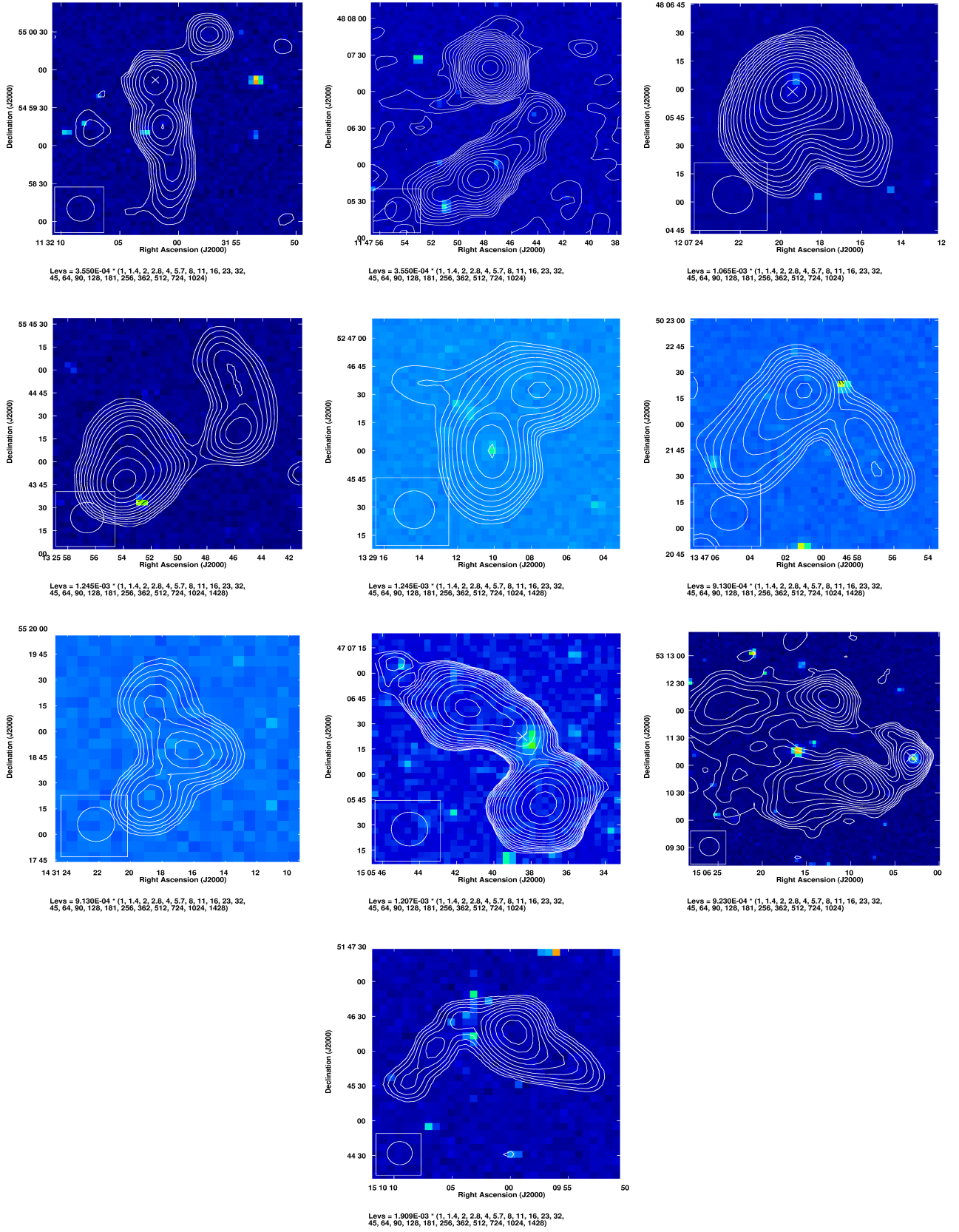


Figure 2. LOFAR images of NAT radio galaxies (contours) overlaid on DSS2 red images (colour). Here white cross mark represent the optical counterpart for the sources, when available.

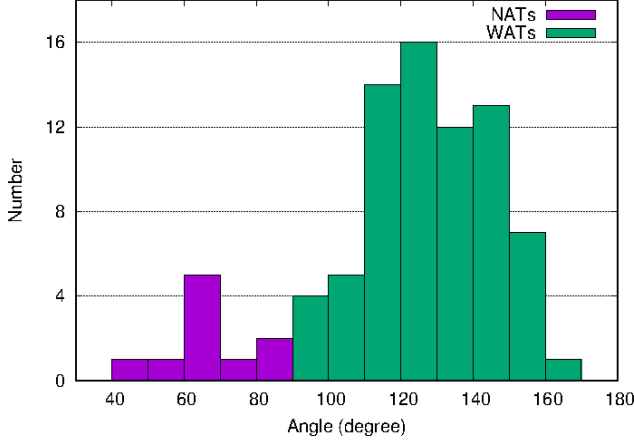


Figure 3. A histogram showing the distribution of bending angle of WATs and NATs presented in the current paper.

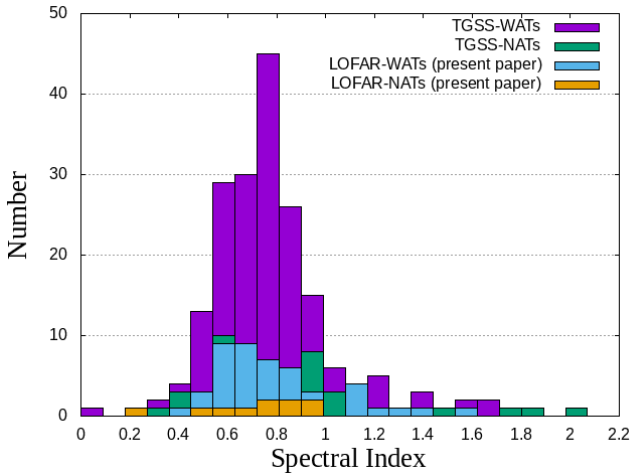


Figure 4. Histogram showing the spectral index (α_{144}^{1400}) distribution of WAT and NAT radio galaxies presented in the current paper.

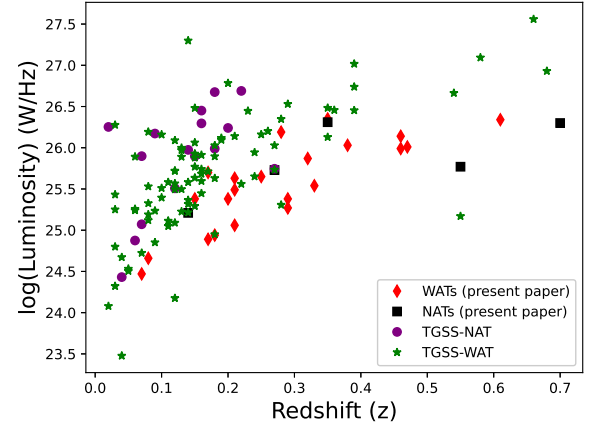


Figure 5. Plot showing the $\log L$ distribution of WAT and NAT radio galaxies with the respected redshift presented in the current paper and Head-Tailed radio galaxies reported by [Bhukta, Pal & Mondal \(2022\)](#). Red diamond color points and black square color points represented WATs and NATs presented in the current paper while purple circle color points and green star color points represented TGSS-NATs and TGSS-WATs.

paper is measured to be 0.78 with a median of 0.75, and the average spectral index for NATs is 0.56 with a median of 0.68. Using a large number (204 WATs and 61 NATs) of HT radio galaxies, [Bhukta, Pal & Mondal \(2022\)](#) found the average spectral index for WATs was 0.77 with a median of 0.73 and for NATs, the average spectral index was 0.81 with a median of 0.73. The spectral index for normal radio galaxies typically lies in the range of 0.7–0.8 ([Oort, Steemers & Windhorst, 1988](#); [Grupponi et al., 1997](#); [Kapahi et al., 1998](#); [Ishwara-Chandra et al., 2010](#); [Mahony et al., 2016](#)). The measured average spectral index for forty-five WAT sources in the present article and 265 sources reported by [Bhukta, Pal & Mondal \(2022\)](#), are close to this range. It can be concluded that in terms of spectral index, HT radio galaxies are similar to those of normal radio galaxies ([Missaglia et al., 2019](#); [Bhukta, Pal & Mondal, 2022](#)). Because of the small number of NATs reported in the current paper (which is not statistically significant), the average spectral index for NATs did not fall within this range.

Radio luminosity is one of the most important properties used to distinguish radio galaxies. In Fig. 5, the distribution of radio luminosity of NATs and WATs is shown for the sources presented in the current paper. 265 sources (204 WATs and 61 NATs) presented by [Bhukta, Pal & Mondal \(2022\)](#) with known red-shift (z) are also added in the figure. It is found that for WAT sources, the mean $\log L_{\text{rad}}$ and median $\log L_{\text{rad}}$ are cal-

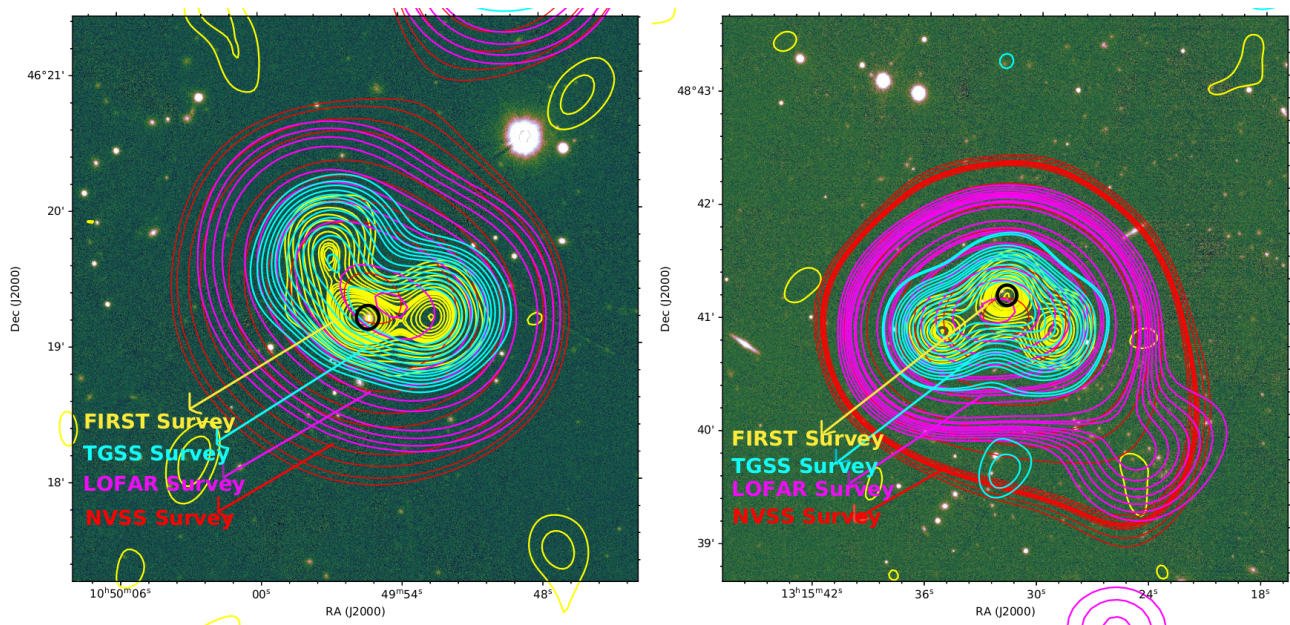


Figure 6. Example of two WAT sources: Overlaid image of J1049+4619 and J1315+4841 with FIRST (yellow color), TGSS (cyan color), LOFAR (magenta color), and NVSS (red color) surveys. The background is in optical wavelength, taken from Pan-STARRS (Panoramic Survey Telescope and Rapid Response System). Black color circle represent the optical host galaxy core.

culated as 25.60 and 25.62, respectively. Similarly, for NAT sources, the mean $\log L_{\text{rad}}$ and median $\log L_{\text{rad}}$ are 25.54 and 25.73, respectively. The mean $\log L_{\text{rad}}$ and median $\log L_{\text{rad}}$ for the HT radio galaxies presented by Missaglia *et al.* (2019) were 25.40 and 25.35, respectively. The mean and median $\log L_{\text{rad}}$ for WAT sources in Bhukta, Pal & Mondal (2022) were 25.62 and 25.63, respectively, and for NAT sources, the mean and median were 25.82 and 25.83, respectively. This result suggests that the average luminosity of WAT and NAT sources in the present paper is more or less the same as that reported by Bhukta, Pal & Mondal (2022) (with the help of TGSS ADR 1 at 150 MHz) and Missaglia *et al.* (2019).

In Fig. 6, we showed the examples of two WAT (J1049+4619 and J1315+4841) sources. We made overlay images of these sources using LOTSS DR1, FIRST, TGSS, and NVSS surveys. Emissions from these sources for the LOTSS survey are visible with a magenta colour contour, and those of FIRST, TGSS, and NVSS are visible with yellow, cyan, and red colour contours, respectively. The optical background of these images is taken from the Pan-STARRS. The bending nature is not evident with NVSS contours due to the poor resolution of the survey. A black circle in the centre of the image represents the core of the host galaxy.

4.2 Association with cluster

A galaxy cluster is a structure composed of hundreds or thousands of gravitationally bound galaxies with masses ranging from 10^{14} – $10^{15} M_{\odot}$ with enormous size (Wen, Han & Liu, 2012). We used the NASA Extragalactic Database (NED) to conduct a 3D search of galaxy clusters for each HT radio galaxy with a search radius of 3 arcmins. From the search results, we chose the clusters that are closest to the HT radio galaxies. Using this method of searching, we found 30 HT radio galaxies (25 are WATs and 5 are NATs) that match known galaxy clusters, as listed in Table 3 and 4. Twenty-three clusters are from the Wen+Han+Liu (WHL) cluster catalog (Wen & Han, 2015), which consists of 158,103 clusters (X-ray frequency). Two clusters are from the Gaussian Mixture Brightest Cluster Galaxy (GMBCG) (Hao *et al.*, 2010) catalog, which consist of 55,880 clusters (optical), 1 from the NSC (Smith *et al.*, 2012) cluster catalog (optical), 1 from MSPM (Smith *et al.*, 2012) cluster catalog (optical), 2 from SDSS-C4-DR3 (Von *et al.*, 2007) cluster catalog (optical), and 1 from MaxBCG (Koester *et al.*, 2007) cluster catalog (optical).

We computed linear distances between HT radio galaxies and their associated known cluster centres. The majority of cluster centres are located within a few kpc and the shortest and longest distances from the host galaxies are 3.84 kpc and 936.80 kpc, respectively, with a median of 41.27 kpc.

4.3 Cluster mass

The density of the inter-cluster medium is correlated with cluster mass, with heavier clusters having a denser inter-cluster medium. The velocity dispersion of HT radio galaxies is also correlated with the mass of the cluster. It is believed that HT radio galaxies show rapid movement in high mass clusters (Mao *et al.*, 2010). We calculated cluster mass M_{500} ($10^{14} M_{\odot}$) for detected associated clusters of the HT sources described in the present paper with the help of cluster richness R_L using,

$$\log M_{500} = (1.08 \pm 0.02) \log R_L - (1.37 \pm 0.02) \quad (3)$$

The cluster richness (R_L) and cluster radius from optical luminosity (r_{500}) of 22 WHL clusters are listed in Table 3 and 4 (taken from (Wen & Han, 2015)).

The mass of the ICM gas that is contained inside a radius of r_{500} is M_{500} , where r_{500} is the radius containing the mean over-density of $\Delta c = 500\rho_{cr}$, where $\rho_{cr}(z) = 3H(z)^2/8\pi G$ is the critical mean density of the universe as defined in terms of the Hubble function $H(z)$. The relative velocities of galaxies are consistent with the temperature of the ICM, which indicates that both galaxies and gas are nearly in equilibrium within a common gravitational potential well. The depth of the potential well cannot be explained by the mass of galaxies and hot gases, suggesting that the majority of the mass in clusters is made up of dark matter.

We reported that 30 out of 55 HT radio galaxies are associated with groups of relatively low mass clusters (in the order of $10^{14} M_{\odot}$). In our catalogue, the most massive cluster associated with a WAT is WHL J145943.2+494716 (with mass (M_{500}) $5.09 \times 10^{14} M_{\odot}$) of which host galaxy is J1459+5334. The most massive cluster associated with a NAT is WHL J145943.2+494716 (with mass (M_{500}) $4.47 \times 10^{14} M_{\odot}$) of which host galaxy is J1505+4706.

In the classification of HT radio galaxies, projection effects may have an impact. Due to projection effects, the large jets (up to a few degrees) of HT radio galaxies that would appear straight in the line of sight are excluded from our sample. The number of observed HT radio galaxies at any given time is also highly dependent on the AGN duty cycle in the formation of bent jets.

The redshifts of the associated cluster are mentioned in Table 3 and 4. These redshifts are taken from NED and SDSS.

5. Summary and Conclusions

In this paper, we report the identification of 55 HT radio galaxies (45 WATs and 10 NATs). The current cata-

logue of 55 newly detected HT radio galaxies will help to increase the number of known HT radio galaxies. Among all 55 HT radio galaxies, SDSS optical counterparts are found for 44 HT radio galaxies. Four sources are reported as possible radio relic sources. Seven sources (four WATs (J1115+4729, J1344+5552, J1431+4743, and J1523+5255) and three NATs (J1329+5246, J1431+5518, and J1325+5544)) have no optical counterparts, and they are also not associated with any galaxy clusters. More in-depth optical follow-up observations are needed to search for possible optical counterparts of these sources. We found that thirty out of the fifty-five HT are linked to known galaxy clusters.

The detection of 55 HT radio galaxies in a 424 square degree area suggests that these types of sources are not uncommon, particularly in cluster-rich areas. Future multi-wavelength follow-up observations with high resolution and high sensitivity surveys, especially using SKA, will be able to detect a large number of HT radio galaxies and will help to understand the nature of these sources in more detail.

Acknowledgments

The LOFAR Two-metre Sky Survey (LoTSS) is being conducted with the high-band antennas (HBA) of LOFAR which is funded by the EU, European Fund for Regional Development and the Northern Netherlands Provinces (SNN), and EZ/KOMPAS and managed by ASTRON Netherlands Institute for Radio Astronomy. This research has made use of the NASA/IPAC Extragalactic Database (NED) which is operated by the Jet Propulsion Laboratory, California Institute of Technology, under contract with the National Aeronautics and Space Administration.

References

- Aghanim N. *et al.*, 2020, A&A, 641, 67
- Agüeros M.A. *et al.*, 2005, AJ, 130, 1022
- Baan W.A., McKee M.R., 1985, A&A, 143, 136
- Becker R.H. *et al.*, 1995, ApJ, 450, 559
- Benn C. R., Grueff G., Vigotti M., Wall J.V., 1982, MNRAS, 200, 747
- Benn C. R., Grueff G., Vigotti M., Wall J.V., 1988, MNRAS, 230, 1
- Bhukta N., Pal S., Mondal S., 2022, MNRAS, 516, 372
- Blanton E.L., Gregg M.D., Helfand D.J., Becker R.H., White R.L., 2000, ApJ, 531, 118
- Blanton E.L., Gregg M.D., Helfand D.J., Becker R.H., White R.L., 2003, AJ, 125, 1635

- Bolton J.G., Gardner F.F., Mackey M.B., 1964, *AuJPh*, 17, 340
- Bonafede A. *et al.*, 2012, *MNRAS*, 426, 40
- Burns J. O., 1998, *Sci*, 280, 400
- Chung S.M., Eisenhardt P.R., Gonzalez A.H., Stanford S.A., Brodwin M., Stern D., Jarrett T., 2011, *ApJ*, 743, 34
- Cohen A.S., Lane W.M., Cotton W.D., Kassim N.E., Lazio T.J.W., Perley R.A. Condon J.J., Erickson W.C., 2007, *AJ*, 134, 1245
- Cordey R. A., 1987, *Monthly Notices of the RAS*, 227, 695
- Condon J.J., Cotton W.D., Greisen E.W., Yin Q.F., Perley R.A., Taylor G.B., Broderick J.J., 1998, *AJ*, 115, 1693
- de Gasperin F. *et al.*, 2015, *MNRAS*, 453, 3483
- Dehghan S., Johnston-Hollitt M., Franzen T.M.O., Norris R.P., Miller N.A., 2014, *AJ*, 148, 75
- Donoso E., Best P. N., Kauffmann G., 2009, *MNRAS*, 392, 617
- Douglas J.N., Bash F.N., Bozayan F.A., Torrence G.W., Wolfe C., 1996, *AJ*, 111, 1945
- Dreyer J.L.E., 1888, *MmRAS*, 49, 1
- Eilek J.A., Burns J.O., O'Dea C.P., Owen F.N., 1984, *ApJ*, 278, 37
- Eilek J.A., Owen F.N., 2002, *ApJ*, 567, 202
- Fernández P.D. *et al.*, 2021, *MNRAS*, 507, 2714
- Ficarra A., Grueff G., Tomassetti G., 1985, *A&AS*, 59, 255
- Gregory P.C., Condon J.J., 1991, *ApJS*, 75, 1011
- Gruppioni C., Zamorani G., de Ruiter H.R., Parma P., Mignoli M., Lari C., 1997, *MNRAS*, 286, 470
- Gunn J. E., Gott J. R. I., 1972, *ApJ*, 176, 1
- Gunn J.E. *et al.*, 2006, *AJ*, 131, 2332
- Hales S.E.G., Baldwin J.E., Warner P.J., 1988, *MNRAS*, 234, 919
- Hales S.E.G., Masson C.R., Warner P.J., Baldwin J.E., 1990, *MNRAS*, 246, 256
- Hales S.E.G., Mayer C.J., Warner P.J., Baldwin J.E., 1991, *MNRAS*, 251, 46
- Hales S.E.G., Baldwin J.E., Warner P.J., 1993a, *MNRAS*, 263, 25
- Hales S.E.G., Masson C.R., Warner P.J., Baldwin J.E., Green D.A., 1993b, *MNRAS*, 262, 1057
- Hao J. *et al.*, 2010, *ApJS*, 191, 254
- Hardcastle M.J., Sakelliou I., Worrall D.M., 2005, *MNRAS*, 359, 1007
- Heald G. H. *et al.* 2015, *A&A*, 582, A123
- Hurley-Walker N., *et al.*, 2015, *MNRAS*, 447, 2468
- Intema H. T., Jagannathan P., Mooley K.P., Frail D.A., 2017, *A&A*, 598, A78
- Ishwara-Chandra C.H., Sirothia S.K., Wadadekar Y., Pal S., Windhorst R., 2010, *MNRAS*, 405, 436
- Kapahi V.K., Athreya R.M., van Breugel W., McCarthy P.J., Subrahmanya C.R., 1998, *ApJS* 118, 275
- Kenderdine S., Ryle M.S., Pooley G.G., 1966, *MNRAS*, 134, 189
- Klamer I., Subrahmanyan R., Hunstead R. W., 2004, *MNRAS*, 351, 101
- Kollgaard R.I., Brinkmann W., Chester M.M., Feigelson E.D., Hertz P., Reich P., Wielebinski R., 1994, *ApJS*, 93, 145
- Koester B. P., McKay T. A. Annis J., Wechsler R. H *et al.*, 2007, *ApJ*, 660, 239
- Lane W.M., Cotton W.D., van Velzen S., Clarke T.E., Kassim N.E., Helmboldt J.F., Lazio T.J.W., Cohen A.S., 2014, *MNRAS*, 440, 327
- Mao M. Y., Sharp R., Saikia D. J., Norris R. P., Hollitt M. J., Middelberg E., Lovell J. E. J., 2010, *MNRAS*, 406, 2578
- Mahony E.K. *et al.*, 2016, *MNRAS*, 463, 2997
- McGilchrist M.M., Baldwin J.E., Riley J.M., Titterton D.J. Waldram E.M., Warner P.J., 1990, *MNRAS*, 246, 110
- Miley G. K., Perola G. C., van der Kruit P. C., van der Laan H., 1972, *Nat*, 237, 269
- Mingo *et al.*, 2019, *MNRAS*, 488, 2701
- Missaglia V., Massaro F., Capetti A., Paolillo M., Kraft R. P., Baldi R. D., Paggi A., 2019, *A&A*, 626, A8
- Murgia M., *et al.*, 2011, *a&a*, 526, A148
- O'Brien A.N. *et al.*, 2018 *MNRAS*, 481, 5247
- O'Dea C.P., Owen F.N., 1986, *ApJ*, 301, 841
- Oort M.J.A., Steemers W.J.G., Windhorst R. A., 1988, *A&AS*, 73, 103
- Owen F.N., Rudnick L., 1976, *ApJ*, 205, L1
- Pal S., Kumari S., 2021, *astro-ph:2104.00410*
- Patra D., Pal S., Konar C., Chakrabarti S.K., 2019, *Astrophys Space Sci*, 364, 72
- Pearson T.J., 1975, *MNRAS*, 171, 475
- Pearson T.J., Kus A.J., 1978, *MNRAS*, 182, 273
- Piffaretti R., Arnaud M., Pratt G. W., Pointecouteau E., Melin J. B., 2011, *A&A*, 534, 109
- Pooley G.G., Kenderdine S., 1968, *MNRAS*, 139, 529
- Pooley G.G., 1969, *MNRAS*, 144, 101
- Proctor D.D., 2011, *ApJS*, 194, 31
- Rebull L.M. *et al.*, 2011, *ApJS*, 196, 4
- Rudnick L., Owen F.N., 1976, *AJ*, 203, L107
- Rudnick L., Owen F. N. 1977, *AJ*, 82, 1

- Ryle M., Windram M.D., 1968, MNRAS, 138, 1
- Sánchez A.J., Aguerri J.A.L., Muñoz-Tuñón C., Huertas-Company M., 2011, ApJ, 735, 125
- Sasmal T.K., Bera S., Pal S., Mondal S., 2022, ApJS, 259, 9
- Schuch N.J., 1981, MNRAS, 196, 695
- Skrutskie M.F. *et al.*, 2006, AJ, 131, 1163
- Shimwell T.W. *et al.*, 2019, A&A, 622, A1
- Smith A.G. *et al.*, 2012, MNRAS, 422, 25
- Tamhane P., Wadadekar Y., Basu A., Singh V., Ishwara-Chandra C. H., Beelen A., Sirothia S., 2015, MNRAS, 453, 2438
- van Weeren R. J., Röttgering H. J. A., Brüggén M., Hoeft M., 2010, Science, 330, 347
- van Weeren, R. J. *et al.*, 2012, MNRAS, 425, L36
- Venkatesan T. C. A., Batuski D. J., Hanisch R. J., Burns J. O., 1994, ApJ, 436, 67
- Vessey S.J., Green D.A., 1998, MNRAS, 294, 607
- Von D.L.A., Best P.N., Kauffmann G., White S.D.M., 2007, MNRAS, 379, 867
- Waggett P.C., 1977, MNRAS, 181, 547
- Waldram E.M., Yates J.A., Riley J.M., Warner P.J., 1996, MNRAS, 282, 779
- Wayth R.B. *et al.*, 2015, PASA, 32, e025
- Wen Z. L., Han J. L., Liu F. S., 2012, ApJS, 199, 34
- Wen Z.L., Han J.L., 2015, ApJ, 807, 178
- Willson M.A.G., 1970, MNRAS, 151, 1
- Willis A. G., Strom R. G., Wilson A. S., 1974, Nature, 250, 625
- Yu-Xing Liu, Hai-Guang Xu, Dong-Chao Zheng, *et al.*, 2019, RAA, 19, 127

Table 1. WAT Radio Sources from LoTSS DR1.

Cat. Num.	Name	R.A. (J2000.0)	Decl. (J2000.0)	Redshift (z)	F_{144} (mJy)	F_{1400} (mJy)	α_{1400}^{144}	$\log L_{\text{rad}}$ (W Hz ⁻¹)	Others Catalog
(1)	(2)	(3)	(4)	(5)	(6)	(7)	(8)	(9)	(10)
W1	J1049+4619	10 49 55.89	+46 19 20.4	0.35	546	109	0.72	26.35	1, 4, 7, 8, 14
W2	J1051+5041	10 51 58.99	+50 41 59.8	–	160	19	0.95	–	1, 5
W3	J1057+4749	10 57 26.97	+47 49 27.4	0.18	96	27	0.57	24.94	1, 9
W4	J1101+5603	11 01 08.50	+56 03 20.6	–	132	17	0.92	–	–
W5	J1105+4800	11 05 04.47	+48 00 43.5	–	60	14	0.65	–	1
W6	J1112+5151	11 12 21.67	+51 51 27.7	–	49	8	0.81	–	1
W7	J1113+4952	11 13 17.60	+49 52 00.2	0.61	169	57	0.49	26.34	1
W8	J1114+4611	11 14 16.50	+46 11 15.1	–	289	26	1.08	–	1, 4
W9*	J1115+4729	11 15 31.64	+47 29 29.7	–	63	15	0.63	–	1
W10	J1115+4834	11 15 41.19	+48 34 19.4	0.07	239	64	0.59	24.47	1, 9
W11	J1120+5308	11 20 40.88	+53 08 09.4	–	60	5	1.11	–	1
W12	J1121+5421	11 21 13.68	+54 21 34.4	0.21	87	15	0.79	25.06	1, 9
W13	J1124+5546	11 24 25.08	+55 46 14.8	–	40	7	0.78	–	1
W14	J1127+5533	11 27 18.40	+55 33 32.8	–	22	5	0.66	–	1
W15	J1147+4917	11 47 51.70	+49 17 31.3	–	55	9	0.81	–	1
W16	J1147+5548 ⁺	11 47 15.68	+55 48 19.4	–	41	6	0.85	–	–
W17	J1154+4949	11 54 12.94	+49 49 01.0	0.29	61	4	1.22	25.27	1
W18	J1208+5458	12 08 05.93	+54 58 07.2	0.46	110	9	1.12	25.99	1
W19	J1220+5334	12 20 50.22	+53 34 33.8	0.21	239	47	0.73	25.49	–
W20	J1224+4905	12 24 12.49	+49 05 51.8	–	198	6	1.57	–	1
W21	J1224+5419	12 24 49.89	+54 19 34.2	0.47	111	9	1.13	26.01	1
W22	J1236+5525	12 36 47.43	+55 25 10.6	0.32	230	61	0.59	25.87	1, 4
W23	J1238+4838	12 38 58.26	+48 38 20.5	0.46	174	25	0.87	26.14	1
W24	J1247+4852	12 47 42.73	+48 52 05.9	0.21	293	15	1.33	25.63	3, 16
W25	J1249+4954	12 49 39.23	+49 54 03.1	–	119	26	0.68	–	1
W26	J1303+4743	13 03 48.51	+47 43 19.4	–	226	42	0.75	–	1, 10
W27	J1303+4935	13 03 27.70	+49 35 56.5	0.25	234	51	0.68	25.65	1
W28	J1303+5220	13 03 32.48	+52 20 10.3	–	108	24	0.67	–	10, 11
W29	J1306+5144	13 06 10.82	+51 44 22.6	0.28	652	180	0.58	26.19	1, 2, 8
W30	J1315+4841	13 15 31.82	+48 41 11.7	–	455	75	0.81	–	1, 4
W31	J1325+5617	13 25 04.38	+56 17 42.3	–	107	43	0.41	–	1
W32	J1330+4730	13 30 32.67	+47 30 55.6	0.33	98	32	0.50	25.54	12
W33*	J1344+5552	13 44 44.58	+55 52 03.3	–	543	166	0.52	–	–
W34	J1346+5250 ⁺	13 46 06.92	+52 50 17.6	–	237	63	0.58	–	1, 17
W35	J1351+5216	13 51 50.83	+52 16 29.7	0.17	87	14	0.82	24.89	1
W36	J1359+4905	13 59 44.53	+49 05 33.7	–	124	23	0.75	–	1
W37	J1426+5547	14 26 06.46	+55 47 26.5	–	89	15	0.80	–	1
W38	J1428+5520	14 28 42.42	+55 20 51.5	0.29	210	51	0.63	25.38	12
W39*	J1431+4743	14 31 50.54	+47 43 57.1	–	255	64	0.61	–	1
W40	J1434+4951	14 34 41.95	+49 51 09.7	0.20	221	49	0.67	25.38	–
W41	J1439+5631	14 39 19.32	+56 31 39.4	–	121	31	0.61	–	12, 15, 16
W42	J1446+4841	14 46 06.73	+48 41 40.0	0.38	205	27	0.91	26.03	1
W43	J1459+4947	14 59 42.61	+49 47 17.5	0.17	630	184	0.55	25.70	1, 2
W44	J1459+5334	14 59 35.96	+53 34 19.8	0.08	262	13	1.35	24.66	1
W45*	J1523+5255	15 23 27.06	+52 55 07.4	–	234	50	0.68	–	1, 16

1. NVSS (Condon *et al.*, 1998); 2. VLSS (Cohen *et al.*, 2007); 3. 5C (Kenderdine, Ryle & Pooley, 1966; Pooley & Kenderdine, 1968; Pooley, 1969; Willson, 1970; Pearson, 1975; Waggett, 1977; Pearson & Kus, 1978; Schuch, 1981; Benn *et al.*, 1982, 1988); 4. 6C (Baan & McKee, 1985), (Hales, Baldwin & Warner, 1988; Hales *et al.*, 1990, 1991, 1993a,b); 5. 7C (McGilchrist *et al.*, 1990; Kollgaard *et al.*, 1994; Waldram *et al.*, 1996; Vessey & Green, 1998); 6. PKS (Bolton, Gardner & Mackey, 1964); 7. TXS (Douglas *et al.*, 1996); 8. 87GB (Gregory & Condon, 1991); 9. ASK (Sánchez *et al.*, 2011); 10. 2MASX (Skrutskie *et al.*, 2006); 11. GALEXASC (Agüeros *et al.*, 2005); 12. GALEXMSC (Agüeros *et al.*, 2005); 13. NGC (Dreyer, 1888); 14. B3 (Ficarra, Grueff & Tomassetti, 1985); 15. WISE (Chung *et al.*, 2011; Rebull *et al.*, 2011); 16. 2MASS (Skrutskie *et al.*, 2006)

NOTE: ‘*’ Sources with no optical counterparts

‘+’ possible radio relic sources

Table 2. NAT Radio Sources from LoTSS DR1.

Cat. Num.	Name	R.A. (J2000.0)	Decl. (J2000.0)	Redshift (z)	F_{144} (mJy)	F_{1400} (mJy)	α_{1400}^{144}	$\log L_{\text{rad}}$ (W Hz ⁻¹)	Others Catalog
(1)	(2)	(3)	(4)	(5)	(6)	(7)	(8)	(9)	(10)
N1	J1132+5459	11 32 01.98	+54 59 51.9	0.55	51	9	0.78	25.77	1
N2	J1147+4805	11 47 48.43	+48 05 49.1	0.70	111	34	0.53	26.30	1
N3	J1207+4805	12 07 19.42	+48 05 58.7	0.35	488	84	0.79	26.31	1, 2
N4*	J1325+5544	13 25 48.42	+55 44 14.7	–	231	35	0.83	–	1, 16
N5*	J1329+5246	13 29 09.51	+52 46 19.9	–	135	19	0.86	–	1
N6	J1347+5022 ⁺	13 47 01.03	+50 22 17.9	–	107	13	0.93	–	1, 17
N7*	J1431+5518	14 31 16.33	+55 18 49.9	–	66	8	0.93	–	1
N8	J1505+4706	15 05 38.47	+47 06 22.4	0.27	264	163	0.22	25.73	1, 16
N9	J1506+5311	15 06 03.10	+53 11 09.3	0.14	299	66	0.68	25.21	1
N10	J1510+5146 ⁺	15 10 03.48	+51 46 28.1	–	198	57	0.55	–	1, 14

1. NVSS (Condon *et al.*, 1998); 2. VLSS (Cohen *et al.*, 2007); 3. 5C (Kenderdine, Ryle & Pooley, 1966; Pooley & Kenderdine, 1968; Pooley, 1969; Willson, 1970; Pearson, 1975; Waggett, 1977; Pearson & Kus, 1978; Schuch, 1981; Benn *et al.*, 1982, 1988); 4. 6C (Baan & McKee, 1985), (Hales, Baldwin & Warner, 1988; Hales *et al.*, 1990, 1991, 1993a,b); 5. 7C (McGilchrist *et al.*, 1990; Kollgaard *et al.*, 1994; Waldram *et al.*, 1996; Vessey & Green, 1998); 6. PKS (Bolton, Gardner & Mackey, 1964); 7. TXS (Douglas *et al.*, 1996); 8. 87GB (Gregory & Condon, 1991); 9. ASK (Sánchez *et al.*, 2011); 10. 2MASX (Skrutskie *et al.*, 2006); 11. GALEXASC (Agüeros *et al.*, 2005); 12. GALEXMSC (Agüeros *et al.*, 2005); 13. NGC (Dreyer, 1888); 14. B3 (Ficarra, Gruelf & Tomasetti, 1985); 15. WISE (Chung *et al.*, 2011; Rebull *et al.*, 2011); 16. 2MASS (Skrutskie *et al.*, 2006)

NOTE: ‘*’ Sources with no optical counterparts

‘+’ possible radio relic sources

Table 3. LoTSS WATs in galaxy clusters.

Source Id	Source Name	Cluster Name	Redshift (z)	Comoving Dist. (Mpc)	Angular Sep. (arcsec)	D_{cl} (kpc)	r_{500} (Mpc)	R_L	M_{500} ($\times 10^{14} M_{\odot}$)	N_{500}
(1)	(2)	(3)	(4)	(5)	(6)	(7)	(8)	(9)	(10)	(11)
1	J1049+4619	WHL J104955.4+461912	0.3508	1426.1	10.38	48.57	0.73	30.58	1.71	13
2	J1057+4749	MSPM 05580	0.0873	378.9	156.24	48.61	–	–	–	–
3	J1112+5151	WHL J111224.7+515414	0.5082	1978.8	167.64	936.80	0.95	69.43	4.16	29
4	J1115+4834	SDSS-C4-DR3 3408	0.0740	323.3	2.70	3.84	–	–	–	–
5	J1121+5421	WHL J112113.6+542133	0.2122	895.1	1.32	4.44	0.68	20.68	1.12	11
6	J1147+5548	WHL J114703.7+554715	0.5650	1916.4	2.00	712.27	0.63	26.71	1.48	9
7	J1154+4949	WHL J115412.9+494858	0.2873	1188.1	4.02	16.65	0.67	21.80	1.19	10
8	J1220+5334	WHL J122051.2+533438	0.2076	876.8	8.94	29.64	0.81	28.83	1.61	18
9	J1224+4905	WHL J122418.6+490550	0.1012	439.2	59.88	112.15	0.64	16.49	0.88	9
10	J1224+5419	WHL J122450.7+541929	0.4672	1839.9	6.06	33.04	0.98	71.72	4.31	29
11	J1236+5525	WHL J123647.3+552511	0.3231	1323.4	1.26	5.62	0.80	32.86	1.85	16
12	J1247+4852	WHL J124743.2+485156	0.2095	884.4	10.74	35.85	0.94	55.86	3.29	37
13	J1249+4954	NSC J124941+495335	0.2542*	1060.5	34.92	133.44	–	–	–	–
14	J1303+4743	GMBCG J195.99926+47.72834	0.3770*	1521.8	116.34	567.24	–	–	–	–
15	J1303+4935	WHL J130327.7+493558	0.2547	1062.5	1.44	5.51	0.66	17.22	0.92	8
16	J1306+5144	WHL J130612.2+514407	0.2773	1149.8	20.22	81.85	0.98	53.93	3.16	28
17	J1315+4841	WHL J131527.6+484025	0.5120	1991.5	62.64	256.38	1.03	81.90	4.97	39
18	J1330+4730	WHL J133032.6+473053	0.3261	1334.6	2.70	12.10	0.72	22.42	1.23	11
19	J1351+5216	WHL J135156.1+521542	0.1653	705.8	67.92	189.85	0.66	20.34	1.10	9
20	J1359+4905	WHL J135949.8+490516	0.1728*	736.4	54.24	156.87	–	–	–	–
21	J1346+5250	MaxBCG J206.50836+52.82084	0.1458*	625.7	76.80	194.51	–	–	–	–
22	J1428+5520	WHL J142843.4+552045	0.2893	1195.7	11.22	46.68	0.66	19.76	1.07	10
23	J1434+4951	GMBCG J218.67368+49.85134	0.2040*	862.4	5.52	18.07	–	–	–	–
24	J1459+4947	WHL J145943.2+494716	0.1705	727.0	6.36	18.20	1.12	83.76	5.09	50
25	J1459+5334	SDSS-C4-DR3 3613	0.0750	327.6	4.14	5.97	–	–	–	–

NOTE: ‘★’ the photometric redshifts

Table 4. LoTSS NATs in galaxy cluster.

Source Id	Source Name	Cluster Name	Redshift (z)	Comoving Dist. (Mpc)	Angular Sep. (arcsec)	D_{cl} (kpc)	r_{500} (Mpc)	R_L	M_{500} ($\times 10^{14} M_{\odot}$)	N_{500}
(1)	(2)	(3)	(4)	(5)	(6)	(7)	(8)	(9)	(10)	(11)
1	J1207+4805	WHL J120719.4+480605	0.3532	1435.0	6.18	29.03	0.68	16.96	0.91	8
2	J1347+5022	WHL J134708.2+502222	0.5746	2196.7	68.70	410.59	0.70	33.36	1.88	10
3	J1505+4706	WHL J150538.1+470617	0.2648	1101.6	6.48	27.35	1.01	74.29	4.47	43
4	J1506+5311	WHL J150602.9+531108	0.1414	607.5	2.64	6.82	0.81	32.89	1.85	20
5	J1510+5146	WHL J151003.4+514612	0.2073	875.6	16.56	54.85	0.84	30.94	1.74	10